Overview of ASDEX Upgrade Results

H. Zohm 1), C. Angioni 1), R. Arslanbekov 1), C. Atanasiu 2), G. Becker 1), W. Becker 1), K. Behler 1), K. Behringer 1), A. Bergmann 1), R. Bilato 1), V. Bobkov 1), D. Bolshukhin 1), T. Bolzonella 3), K. Borrass 1), M. Brambilla 1), F. Braun 1), A. Buhler 1), A. Carlson 1), G.D. Conway 1), D. P. Coster 1), R, Drube 1), R. Dux 1), S. Egorov 4), T. Eich 1), K. Engelhardt 1), H.-U. Fahrbach 1), U. Fantz 5), H. Faugel 1), K.H. Finken 6), M. Foley 7), P. Franzen 1), J. C. Fuchs 1), J. Gafert 1), K.B. Fournier 8), G. Gantenbein 9), O. Gehre 1), A. Geier 1), J. Gernhardt 1), T. Goodman 10), O. Gruber 1), A. Gude 1), S. Günter 1), G. Haas 1), D. Hartmann 1), B. Heger 5), B. Heinemann 1), A. Herrmann 1), J. Hobirk 1), F. Hofmeister 1), H. Hohenöcker 1), L. D. Horton 1), V. Igochine 1), A. Jacchia 11), M. Jakobi 1), F. Jenko 1), A. Kallenbach 1), O. Kardaun 1), M. Kaufmann 1), A. Keller 1), A. Kendl 1), J.-W. Kim 1), K. Kirov 1), R. Kochergov 1), H. Kollotzek 1), W. Kraus 1), K. Krieger 1), T. Kurki-Suonio 12) B. Kurzan 1), P. T. Lang 1), C. Lasnier, 8), P. Lauber 1), M. Laux 1), A.W. Leonard 13), F. Leuterer 1), A. Lohs 1), A. Lorenz 1), R. Lorenzini 3), C. Maggi 1), H. Maier 1), K. Mank 1), M.-E. Manso 14), P. Mantica 12), M. Maraschek 1), E. Martines 3), K.-F. Mast 1), P. McCarthy 7), D. Meisel 1), H. Meister 1), F. Meo 1), P. Merkel 1), R. Merkel 1), D. Merkl 1), V. Mertens 1), F. Monaco 1), A. Mück 1), H. W. Müller 1), M. Münich 1), H. Murmann 1), Y.-S. Na 1), G. Neu 1), R. Neu 1), J. Neuhauser 1), F. Nguyen 15), D. Nishijima 1), Y. Nishimura 1), J.-M. Noterdaeme 1), I. Nunes 14), G. Pautasso 1), A. G. Peeters 1), G. Pereverzev 1), S. D. Pinches 1), E. Poli 1), M. Proschek 16), R. Pugno 1), E. Quigley 7), G. Raupp 1), M. Reich 1), T. Ribeiro 14), R. Riedl 1), V. Rohde 1), J. Roth 1), F. Ryter 1), S. Saarelma 12), W. Sandmann 1), A. Savtchkov 6), O. Sauter 10), S. Schade 1), H.-B. Schilling 1), W. Schneider 1), G. Schramm 1), E. Schwarz 1), J. Schweinzer 1), S. Schweizer 1), B. D. Scott 1), U. Seidel 1), F. Serra 14), S. Sesnic 1), C. Sihler 1), A. Silva 14), A. C. C. Sips 1), E. Speth 1), A. Stäbler 1), K.-H. Steuer 1), J. Stober 1), B. Streibl 1), E. Strumberger 1), W. Suttrop 1), A. Tabasso 1), A. Tanga 1), G. Tardini 1), C. Tichmann 1), W. Treutterer 1), M. Troppmann 1), H. Urano 1), P. Varela 14), O. Vollmer 1), D. Wagner 1), U. Wenzel 1), F. Wesner 1), E. Westerhof 17), R. Wolf 1), E. Wolfrum 1), E. Würsching 1), S.-W. Yoon 1), Q. Yu 1), D. Zasche 1), T. Zehetbauer 1), H.-P. Zehrfeld 1)

1) Max-Planck-Institut für Plasmaphysik, Garching, Germany, EURATOM Association
2) Institute of Atomic Physics, Romania, EURATOM Association
3) Consorzio RFX, Padova, Italy, EURATOM Association
4) Technical University, Plasma Physics Department, St. Petersburg, CIS
5) University of Augsburg, Germany
6) Institut fr Plasmaphysik, FZ Jülich, Germany, EURATOM Association
7) Physics Department, University College Cork, Association EURATOM-DCU, Ireland
8) Lawrence Livermore National Laboratory, Livermore, USA
9) Institut für Plasmaforschung, Stuttgart University, Germany
10) CRPP, Ecole Polytechnique Federale de Lausanne, Switzerland, EURATOM Association
11) IFP Milano, Italy, EURATOM Association
12) Helsinki University of Technology, Finland, EURATOM Association
13) General Atomics, San Diego, USA
14) Centro de Fusao Nuclear, IST Lisbon, Portugal, EURATOM Association
15) CEA Cadarache, France, EURATOM Association
16) Institute for Applied Physics, Vienna, Austria, EURATOM Association
17) FOM Rijnhuizen, The Netherlands, EURATOM Association

e-mail contact of main author: zohm@ipp.mpg.de

Abstract Recent results from ASDEX Upgrade are presented. An improved understanding of energy and particle transport emerges in terms of a 'critical gradient' model for the temperature gradients. Coupling this to particle diffusion explains most of the observed behaviour of the density profiles, in particular the finding that strong central heating reduces the tendency for density profile peaking. Internal transport barriers with T_e and T_i in excess of 20 keV (but not simultaneously) have been achieved. By shaping the plasma, a regime with small type II ELMs has been established. Here, the maximum power deposited on the target plates was greatly reduced at constant average power. Also, an increase of the ELM frequency by injection of shallow pellets was demonstrated. ELM free operation is possible in the QH-mode regime previously found in DIII-D which has also been established on ASDEX Upgrade. Regarding stability, a regime with benign NTMs was found. During ECCD stabilisation of NTMs, β_N could be increased well above the usual onset level without a reappearance of the NTM. ECRH and ECCD have also been used to control the sawtooth repetition frequency at a moderate fraction of the total heating power. The inner wall of the ASDEX Upgrade vessel has increasingly been covered with tungsten without detrimental effects on plasma performance. Regarding scenario integration, a scenario with a large fraction of noninductively driven current ($\geq$ 50%), but without internal tranport barrier has been established. It combines improved confinement ($\tau_E/\tau_{ITER98} \approx 1.2$) and stability ($\beta_N \leq 3.5$) at high Greenwald fraction ($n_e/n_{GW} \approx 0.85$) in steady state and with type II ELMy edge.

1. Introduction

The ASDEX Upgrade tokamak programme [1] focuses on the preparation of ITER. This includes the investigation of the physics of the baseline ELMy H-mode scenario, as well as the preparation of 'Advanced Scenarii' with performance exceeding that of the ELMy H-mode and a major fraction of noninductively driven current. The underlying physics areas studied are transport of energy and particles, operational boundaries due to MHD instabilities and exhaust of energy and particles by a poloidal divertor. In addition, a number of technological issues related to the heating, fuelling and exhaust systems are resolved. In particular, a strong emphasis is laid on W as wall material.

In this paper, we summarise the progress made with these studies in the 2001 and 2002 experimental campaigns. The results described confirm the viability of the conventional scenario for ITER. The progress made with advanced scenarii shows that also a significant improvement of performance with respect to the standard scenario may be possible in ITER.

2. Upgrade of technical systems

A major change was the redirection of one of the two NBI boxes to provide off-axis deposition with fairly tangential beams [2]. Fig. 1 a) shows the geometry. With 5 MW at 93 keV, it was possible to show significant current drive by NBI. Fig. 1 b) shows a comparison of two discharges: in #15884, off-axis beams were used, in #15887, on-axis beams were applied. Both discharges have similar T_e, n_e and Z_{eff} profiles, und thus equal electrical resistance. With off-axis NBI, the consumption of OH flux is reduced, as can be seen by the difference in OH current ramp. While the magnitude of the driven current is in reasonable agreement with the theoretically expected value, the expected change of the current profile is not confirmed by the MSE measurements. Such an effect could be due to an anomalous radial diffusion of the fast NBI particles. Further studies will have to clarify this effect.

After a refurbishment of the ICRH generator tubes and with the use of 3 dB couplers minimising the effect of reflected ICRH power onto the generators, reliable ICRH operation even in type I ELMy H-mode was achieved with power levels up to 7.2 MW (90 % of the generator power) at the antennas. Also, we have validated ion cyclotron heating at the 3/2 resonance frequency using a two-species (D and H) plasma in which a fast wave excites an ion Bernstein wave in the centre by mode conversion [3].

The outer divertor leg of the ASDEX Upgrade divertor was rebuilt to accommodate all triangularities with good pumping and power handling. This opened up the operational space at higher

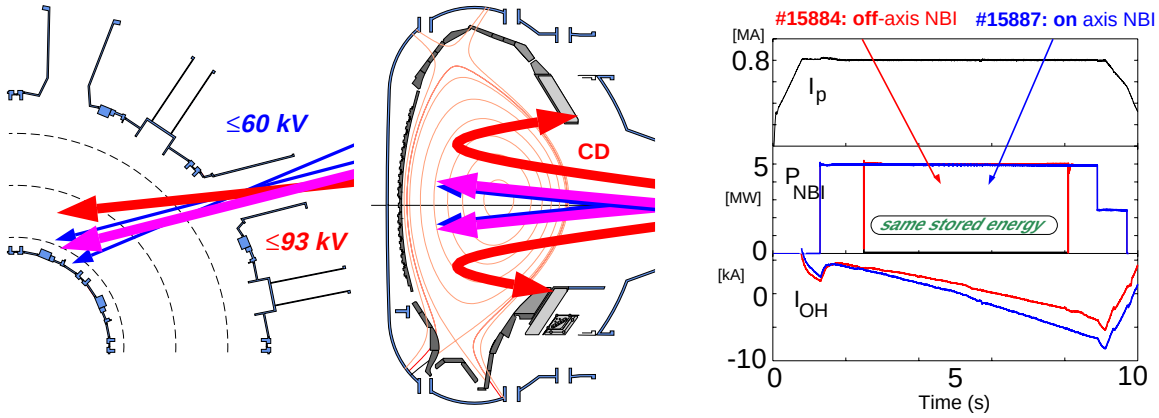

FIG. 1: *Geometry of the ASDEX Upgrade NBI system (left) and comparison of two discharges with on-axis and off-axis NBI. The case with off-axis NBI has lower OH flux consumption, proving the higher NBI driven current in this case.*

triangularity δ up to $\delta = 0.5$, which had a positive impact on confinement and high densities as well as power exhaust with small (type II) ELMs (see section 4). Also, more and more tiles on the inner heat shield were covered successively with a W-coating in order to advance towards a C-free interior of the machine (see section 5). Finally, improvements in the tokamak power supply led to an increase in pulse length; now, 10 s I_p flattop are possible, exceeding the current redistribution time and therefore providing the possibility to study steady state issues even on this timescale. In the coming campaign, even higher $\delta \leq 0.6$ will be possible.

3. Transport studies

Energy transport in conventional scenarii: A major finding in the last years was the observation of 'stiff' T_e and T_i profiles, i.e. a fixed ratio between central T and edge T. This was explained by 'critical gradient' models, that predict the onset of turbulence (ITG, ETG, TEM) below a critical value of the normalised temperature gradient length $L_T = T/\nabla T$ [4]. Using ECRH, it was verified that an electron heat conductivity of the generic form

$$\chi_e = \chi_{e0} + q\lambda T_e^{3/2}(1/L_{T_e} - (1/L_{T_e})_{crit})H(1/L_{T_e} - (1/L_{T_e})_{crit}) \qquad (1)$$

where H is the Heaviside function, explains the experimental observation very well. In particular, it resolves the issue of different values of χ_e from power balance and heat pulse analysis. Fig. 2 shows results from an experiment where the location of the ECRH deposition was varied over the minor radius, keeping the total power constant. This allows us to vary the local heat flux by up to an order of magnitude with unchanged edge T_e. The ECRH power was also modulated to infer the heat pulse χ_e. The parameters $(1/L_{T_e})_{crit}$ and λ in Eqn. (1) were fitted to the power balance data (χ_{e0} is very small and set to zero in the fit). This set of parameters also describes very well the results for the heat pulse $\chi_{e,HP}$ which can be derived from Eqn. (1) by $\chi_{e,HP} = \chi_e + (\partial\chi_e/\partial\nabla T_e)\nabla T_e$ [6].

These experiments demonstrate that the T_e profiles are moderately stiff: for finite central heating, the experimentally measured $1/L_{T_e}$ is in general above $(1/L_{T_e})_{crit}$, i.e. $1/L_{T_e}$ is usually situated somewhat above the marginal point for turbulence onset [5], in good agreement with recent modelling using the Weiland ITG/TEM model [7]. As shown in Fig. 2, in the off-axis case the T_e profile is very close to the threshold in the inner part. This allows us to measure directly the threshold which is in good agreement with that derived for TEM whereas that for ETG is higher by a factor of about 2.

Particle transport: Since the T profiles in general exhibit the 'stiff' behaviour described above, a given pedestal T implies a certain central T. However, n profiles are in general not stiff. It

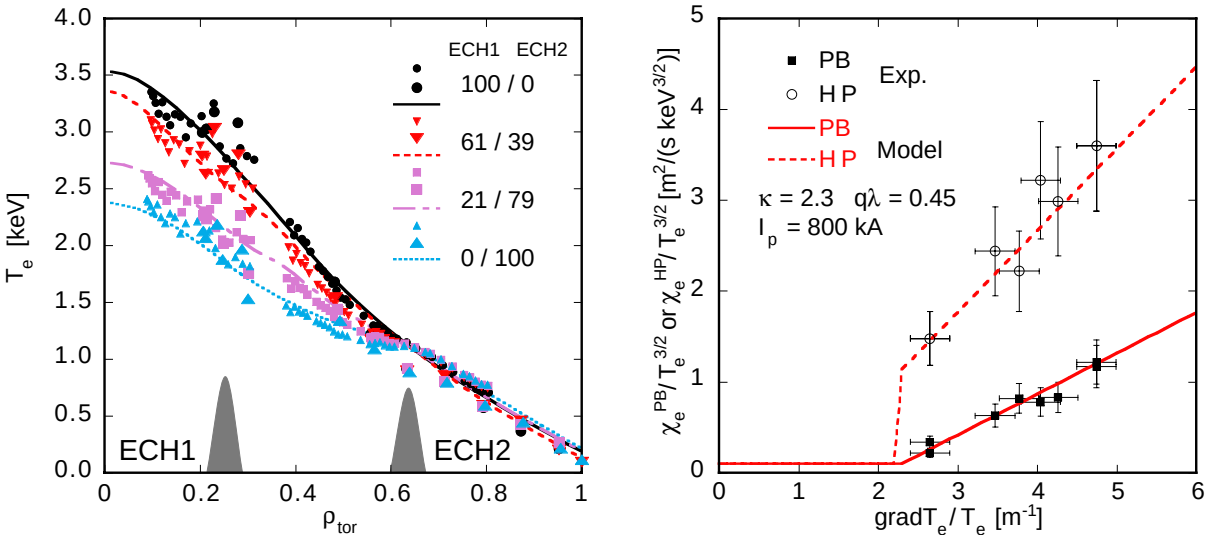

FIG. 2: *T_e profiles from a series of experiments with constant heating power, but varying power fraction between two different locations (left). The variation of local heat flux provides a series of points for analysis of χ_e from power balance and from modulation experiments well described by the simple model from Eq. (1). The analysis is done at* $\rho = 0.5$.

was shown that on ASDEX Upgrade, density peaking occurs on a time scale much longer than the energy confinement time. This can well be described by an inward pinch of the order of the neoclassical Ware pinch in combination with a fixed ratio of the particle diffusion coefficient D to the heat conductivity χ [8]. This model also explains the experimental finding that the density peaking observed with off-axis heating vanishes when the heating power is applied in the centre. Fig. 3 shows a comparison of two discharges where the ICRH deposition is varied and a reference NBI discharge.

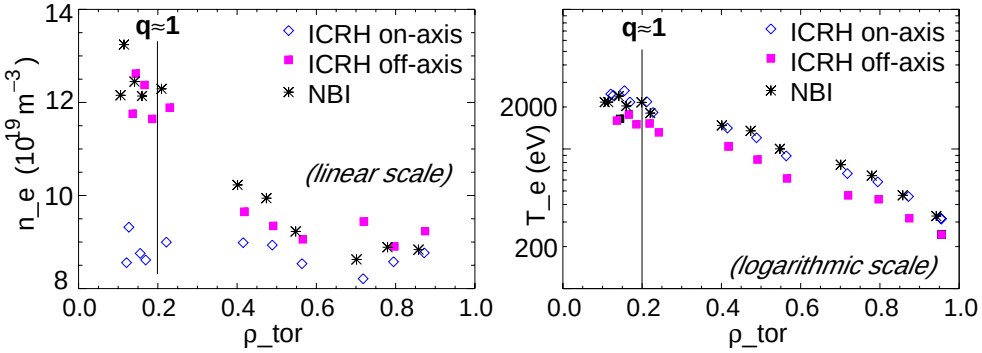

FIG. 3: *T_e and n_e profiles for discharges heated with on-axis ICRH, off-axis ICRH and NBI with off-axis deposition. Since T_e profiles are similar, the centrally heated case has higher central χ_e and thus also higher D, leading to enhanced central particle transport.*

As can be seen, central deposition leads to a much flatter n_e profile, consistent with the interpretation that the central heating power drives the turbulence stronger there (as is expected from the critical gradient model) and thus, through $\chi \propto D$, also the particle transport increases and dominates the inward pinch. This mechanism may also explain the so-called 'ECRH-pumpout', i.e. strongly increased particle transport in the presence of ECRH [9].
Central heating by ICRH and ECRH has also successfully been applied to avoid impurity accumulation that can be observed with reduced central heating[10]. This can be explained by

neoclassical particle transport since a peaked main ion profile can lead to much stronger peaked impurity profiles. A quantitative analysis shows good agreement between neoclassical predictions and experimental results for ASDEX Upgrade [11]. If, under these circumstances, some central heating is applied, impurity accumulation can be completely suppressed. For example, the W-concentration in the centre can be reduced by two orders of magnitude with only 0.8 MW of ECRH in a discharge heated with 5 MW of NBI.

H-mode barrier and pedestal physics: The transport studies described above give a quantitative understanding of the T and n profiles for given pedestal values. However, the understanding of the H-mode pedestal itself is less developed. It had been found before that ∇p in the pedestal region is roughly consistent with the ideal ballooning limit. However, this is a limit to ∇p, but does not discriminate between ∇T and ∇n. Recently, we have found that T_e and n_e profiles in the pedestal region are closely coupled by the relation $\eta_e = d(\log T_e)/d(\log n_e) = 2$, i.e. $T_e = c \times n_e^2$ where c is spatially constant [12], but varies with plasma parameters such as I_p, B_t or the neutral density etc [13]. For known c, this relation, together with the ballooning constraint, determines the profiles in the pedestal region.

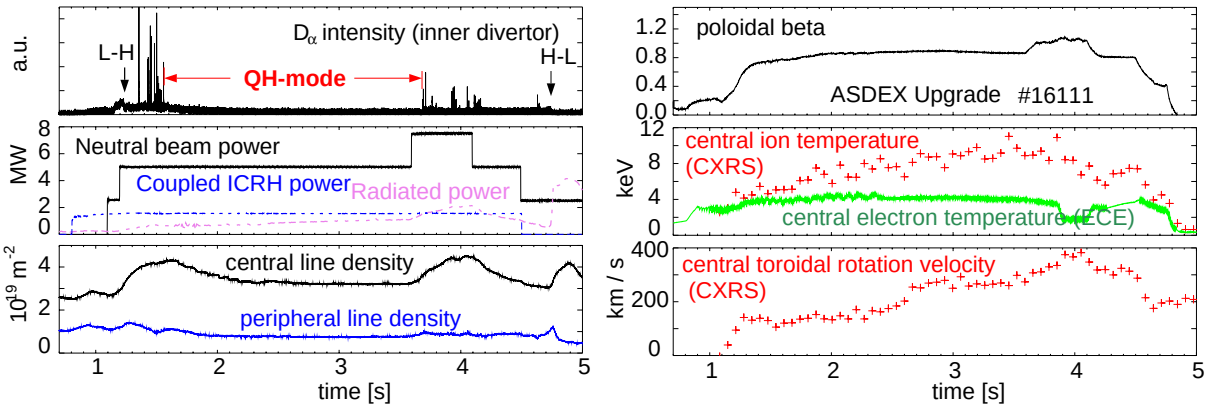

FIG. 4: *Typical QH mode discharge in ASDEX Upgrade with an ELM-free phase of more than two seconds.*

During a campaign with reversed I_p (i.e. counter NBI), it was possible to reproduce the completely ELM-free quiescent H-mode (QH-mode) regime previously found in the DIII-D tokamak [14]. Crucial elements to access the regime were counter NBI, low density and a 'high clearance' (i.e. large plasma-wall distance) equilibrium. Fig. 4 shows a typical example with an ELM-free period of more than 2 seconds in steady state [15]. Consistent with the DIII-D results, an Edge Harmonic Oscillation (EHO) was observed instead of the ELM activity. Details on this mode can be found in section 4.1. However, due to the very low n_e needed to access this regime, Z_{eff} was quite high in spite of the addition of ICRH which prevented accumulation of impurities. Further experimental work has to clarify the relevance of this regime.

Internal transport barriers (ITBs): Concerning ion ITBs, we changed the scenario from an inner wall or upper single null scenario to lower single null operation. The previous scenarii had been chosen because the discharge stayed in L-mode, which was necessary to avoid disruptions due to external kinks that occurred when an ITB discharge transited into H-mode. In the recent campaign, it was found that ITBs could be produced with an H-mode edge without disruptions when the onset of the NBI heating was slightly delayed. A detailed analysis shows that under these circumstances, the target density was lower, which seems to be a decisive parameter for ITB formation in ASDEX Upgrade [16]. Also, the q-profile has more time to relax and may be less inverted than previously; this would be a possible explanation for the absence of the external kink in the new scenario. Unfortunately, due to technical problems, no MSE measurements were

available in the recent campaign to validate this hypothesis.
In ITB discharges with H-mode edge, the ITB phase is accompanied by an ELM-free phase in which the stored energy increases almost linearly without an apparent MHD limit to the central pressure until the first ELM. This first ELM usually also affects the plasma centre and thereby terminates the ITB. The duration of the ELM free phase is almost independent of heating power and the edge ∇p saturates early on in this phase; a possible explanation is that the edge ∇p is limited by a more benign MHD instability and only after the build up of sufficient bootstrap current in the edge does the first ELM occur. Fig. 5 shows an example.

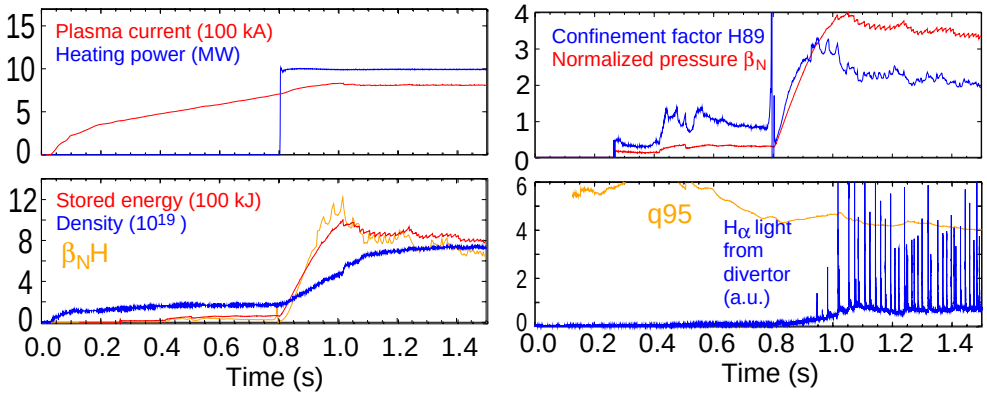

FIG. 5: *ITB discharge with H-mode edge reaching transiently* $\beta_N = 4$ *and* $H_{89} = 3$. *The first ELM ends the high performance phase.*

Concerning ITB physics, a clear reduction of turbulence within the ITB and at its foot point has been found using reflectometry, although the turbulence level does not go down to the diagnostic noise level at low frequencies, indicating that not all modes are suppressed [17]. A further point of interest is the observation that the foot point of the ITB is usually located just outside the shear reversal zone and the steep gradient zone then extends across this zone [16]. This is of particular importance concerning the prospects for stationarity of an ITB discharge with large bootstrap current, since a location of the foot point inside the shear reversal zone would point to a tendency for the ITB to shrink in time.
While the results mentioned so far mainly concern pronounced ion ITBs, we have also made progress in establishing electron ITBs with ctr-ECCD. Previously, it had been found that ctr-ECCD could lead to strong electron ITBs, but the ITBs had a tendency to collapse. By using higher I_p and n_e (i.e. a smaller fraction of driven current), it has been possible to sustain the duration of the ITB phase and reach T_e values in excess of 20 keV [16].

4. MHD Stability

Edge Localised Modes (ELMs): A major programmatic point on ASDEX Upgrade is the preparation of H-mode scenarii with tolerable ELMs, since extrapolations for the transient power loads onto the ITER divertor due to regular type I ELMs give rise to concerns. One way to accomplish this is the operation with type II ELMs [18]. The operational space for type II ELMs in ASDEX Upgrade is characterised by high δ, closeness to double null and high density. Recent studies indicate that closeness to double null is required, whereas the constraint of high δ, which is to some extent coupled to the closeness to double null in ASDEX Upgrade, has recently been reduced to $\langle\delta\rangle \geq 0.35$. Also, the type II operational space is characterised by somewhat elevated q_{95} with respect to the ITER value, but has been extended down to $q_{95} = 3.5$ when operated close to double null. MHD stability analysis has shown that in the type II ELM configuration, the peeling-ballooning stability for lower mode numbers is improved and also, the width of the eigenfunction for given n decreases due to the higher edge shear [20], [21].

Both effects have a tendency to lead to smaller ELMs.
Another regime with small ELMs is the EDA-regime found on ALCATOR C-Mod [22]. Experiments to establish dimensionless similar discharges between ASDEX Upgrade and C-Mod have been performed; however, they are complicated by the fact that the H-mode is not accessible in the dimensionless similar ASDEX Upgrade discharge and, at the higher heating power required in ASDEX Upgrade, ELM-free phases or type I ELMs occur [23]. This will require further studies, in particular because, in JET-ASDEX Upgrade similaritiy experiments, the L-H threshold has been found scale in dimensionless similar variables [24].
Experiments were also performed to increase the type I ELM frequency by injection of shallow pellets that have little effect on n_e, but instantaneously trigger a type I ELM. It could be shown that, by injecting pellets at a frequency higher than the natural type I ELM frequency, the ELM frequency could be significantly increased [25]. Since the ELM energy loss associated with these ELMs is consistent with the scaling derived from variation of the natural ELM frequency ($\nu_{ELM} \times \delta W \approx const.$ at constant P_{heat}), this may open a route to mitigation of the peak heat loads for given heating power.

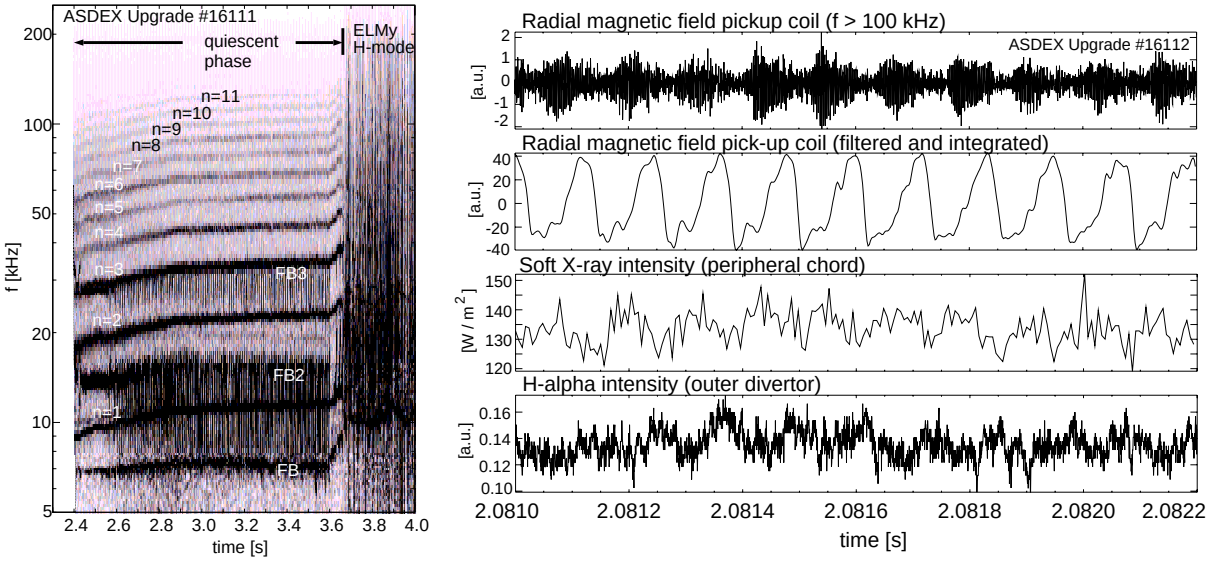

FIG. 6: *Edge harmonic oscillation in QH-mode. The low frequency mode shows harmonics up to* $n = 11$ *(left part, fishbone activity and its harmonics are also seen, marked 'FB'). The right part shows that this is correlated with high frequency bursts transporting particles across the separatrix.*

As mentioned above, the ELM-free quiescent H (QH)-mode regime was established on ASDEX Upgrade. The Edge Harmonic Oscillation (EHO) that was found to be characteristic for this regime in DIII-D is also observed in ASDEX Upgrade during the ELM-free phase. Fig. 6 shows an example where up to the 11th harmnonic can be seen in the spectrum of a Mirnov coil. A feature previously not seen is shown on the right hand side of Fig. 6. Here, data acquired from magnetic coils with a very high frequency response up to 1 MHz and sampled at 2 MHz are shown together with the envelope of the EHO. Note the strongly nonsinusoidal character of the radial magnetic field oscillation which points to a poloidally localised structure, consistent with the existence of many harmonics. As can be seen, each cycle of the EHO coincides with a high-frequency burst at 350-400 kHz. The burst frequency actually decreases in time and therefore points to a fast particle drive of these oscillations. It is at present not clear, how this high frequency oscillation is linked to the EHO, but its high frequency seems to be related to the EHO frequency [15]. However, a role of fast particles in the EHO physics might explain

why it is found only at low density and with ctr-NBI, where first orbit losses are much higher than in the co-case.

Neoclassical Tearing Modes (NTMs): ASDEX Upgrade continues to study ways to avoid, remove or mitigate the effects of NTMs. Previous experiments demonstrated the possibility to stabilise NTMs with DC co-ECCD, but without full confinement and β recovery if the NBI power was kept constant [26]. Now, with higher NBI power, β_N could be significantly increased above the NTM onset level without reappearance of the mode [27]. In addition, the confinement properties of the discharge recover to the value before NTM onset. However, this may be due to the use of the off-axis NBI sources which have a tendency to produce peaked density profiles [2] and therefore counteract the confinement degradation by ECRH. An example is shown is Fig. 7. At even higher β_N, the NTM reappeared in spite of the ECCD; however, this may be due to a mismatch between deposition and island due to the higher Shafranov shift and calls for feedback controlled deposition which will become possible in the near future.

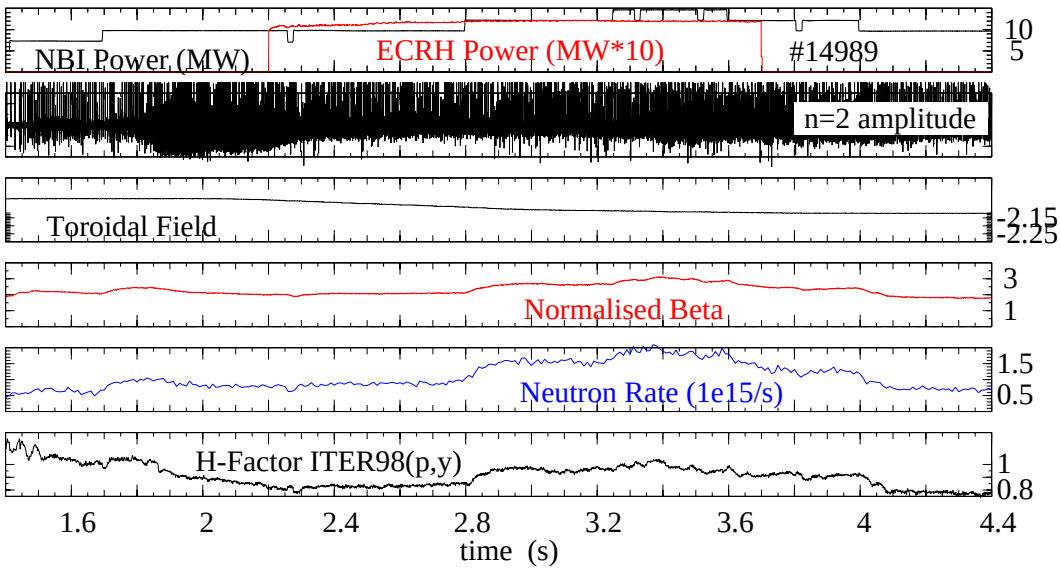

FIG. 7: *NTM stabilisation by DC ECCD. With increased NBI power,* β_N *can be raised significantly above the onset value and confinement recovers.*

An interesting finding concerning NTMs was the discovery of the so-called FIR (Frequently Interrupted Regime) NTMs, in which, for sufficiently high β, an (m,n) NTM never reaches its saturated island width because it is periodically reduced due to interaction with a $(m+1,n+1)$ mode [28], [29]. In this regime, the confinement reduction due to the NTM is significantly reduced and it may be a possible operating regime with tolerable NTMs.

It was found that in discharges with peaked n_e profile, the NTM onset β is unusually low, which may be explained by the fact that ∇n contributes more strongly to the bootstrap current than ∇T [30]. This effect has now been included in the NTM onset scalings by using $(2/3T\nabla n + 1/3n\nabla T)/\nabla p$ rather than β_N in the evaluation of the perturbed bootstrap that drives the mode. Also, experiments were carried out where the heating power was ramped down in order to determine β when the mode is turned off [31], [32]. A marked hysteresis exists between the onset and the switch-off, but the previously found ρ^*-dependence still holds.

Sawtooth tailoring with ECRH: Sawteeth play a key role in determining the central confinement of energy and particles [33]. On the one hand, a loss of sawteeth leads to improved confinement, on the other hand, it may lead to intolerably high central impurity concentrations. Therefore, a method to tailor the sawtooth amplitiude and repetition frequency is highly desirable. This has special importance in the presence of fast particles, that act on sawtooth stability

themselves. Experiments were conducted in ASDEX Upgrade in which 0.8 MW of ECRH power was applied to an H-mode discharge heated with 5 MW of NBI. The ECRH deposition was varied by slow ramps of the toroidal field. The results are summarised in Fig. 8.

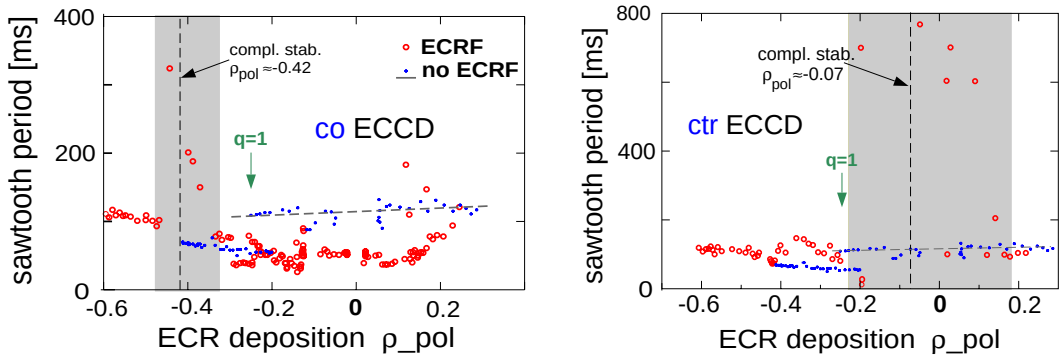

FIG. 8: *Sawtooth repetition period as a function of the ECCD deposition (negative values of* ρ *indicate deposition on the HFS). Complete stabilisation can be achieved by co-ECCD outside the inversion radius or central ctr-ECCD.*

It can be seen that co-ECCD leads to an increase in the sawtooth period when deposited just outside the sawtooth inversion radius. With 800 kW of ECRH/ECCD, it is actually possible to completely stabilise the sawteeth under these circumstances. For central deposition, a reduction in sawtooth period occurs. Similar behaviour is observed with pure ECRH, which is consistent with a local decrease of resistivity due to ECRH that also generates co-current. Conversely, for ctr-ECCD, central deposition stabilises the sawteeth, clearly demonstrating the importance of the local current generated by ECCD. These findings are consistent with the hypothesis that a decrease in current density gradient at the $q = 1$ surface tends to stabilise sawteeth. Note that, contrary to stabilisation of sawteeth by fast particles, the amplitude does not increase here. This method has already been used to create sawtooth-free discharges for impurity transport investigations; future studies will also study the effect of sawtooth tailoring on NTM onset by affecting the seed island size.

Disruptions: Disruptions continue to be an important point of investigation on ASDEX Upgrade. A major concern for ITER are the forces connected with halo currents induced by the movement of a vertically unstable plasma during a disuption. On JET, it had been found that a large asymmetric radial force component can occur during disruptions that can considerably shift the vacuum vessel horizontally. On ASDEX Upgrade, careful measurements were performed to see if this also occurs, but the lateral forces were found to be only a minor fraction of the vertical forces occuring during a disruption [34]. Thus, it has not been possible yet to establish a connection between lateral force and the toroidal asymmetry in halo current that is usually measured in ASDEX Upgrade.

Experiments on disruption mitigation focused on the application of an impurity gas puff as an alternative to the previously used 'killer' pellet. With 120 mbarℓ of Ne injected into a disruption, the forces were reduced up to roughly a factor of 3 due to the faster I_p decay and the smaller vertical displacement which reduce the halo currents. Thus, Ne gas injection is an attractive alternative to a killer pellet.

5. Exhaust and Plasma Wall Interaction

Operation with Divertor IIb: As mentioned above, the outer leg of the ASDEX Upgrade divertor was redesigned to accomodate higher δ plasmas with good pumping and power handling capability. The design principle that had led to the previous Divertor II design was kept: vertical targets with close baffling ensure high divertor density and thus enable strong radiative losses from this region, mainly due to C radiation. Consequently, it was found that the power handling

capability of Divertor IIb is as good as that of its predecessor [35]: although a somewhat higher heat flux to the target plates is observed in Divertor IIb under similar plasma conditions, this can be attributed to the changed geometry that leads to a reduction of the wetted surface due to a steeper field line intersection angle. In fact, by correcting these effects and calculating the parallel heat flux, we arrive at very similar values for Divertor II and Divertor IIb.
Another important property of the divertor is its pumping capability. Comparison between the old and new configuration show only a modest change in the He compression, i.e. the favourable properties of Divertor II were preserved [35]. The new Divertor IIb exhibits the same favourable properties as its predecessor, but allows for more flexibility in plasma shaping which has become increasingly important for many aspects.
Tungsten as first wall material: Recent results on the co-deposition of T in C plasma facing components have drawn increasing attention to alternative wall materials. In 1996, ASDEX Upgrade had been successfully operated with a W-divertor. However, C as the main impurity prevailed, pointing towards a significant role of the C-covered inner heat shield as an impurity source. Thus, we started to successively cover the inner heat shield tiles with W. Operation with up to 7.1 m^2 of the 8.2 m^2 of the inner heat shield covered with W has, under routine operation conditions, not shown any detrimental effect. In particular, the W-concentration rarely exceeded 10^{-5}, which is the critical number for ITER. Conditions in which this number was exceeded were either related to direct contact of the plasma with the inner wall or conditions in which the electron density showed a strong tendency to peak, such as with low central heating. As has been mentioned above, in these cases, addition of central heating led to a large reduction of the central W-concentration [10].
Erosion of W from the inner heat shield showed a pronounced asymmetry over the tiles that led to the conclusion that it is mainly due to ion bombardment (i.e. D and impurities) which, due to the guiding of the particles by the magnetic field, can lead to shadowing of certain areas [36]. This demonstrates that plasma reaches far across the separatrix, a fact that also manifests in the observation of two different decay lengths of the SOL density. This may be due to the bursty nature of SOL transport [12].

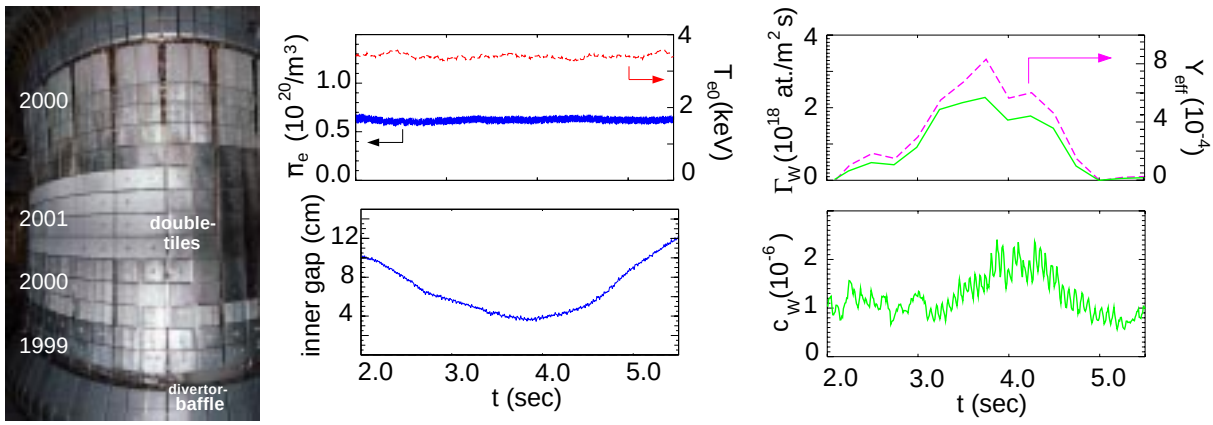

FIG. 9: *Inner wall with W-coated tiles (left) and traces from an experiment where the plasma was brought near the inner wall to determine the relation between W-influx and W-content. The position scan does not influence gobal plasma parameters such as n_e, T_e.*

Fig. 9 shows a view of the inner heat shield covered with W-coated tiles. Also shown are traces from an experiment where the plasma was moved towards the central column and then away from it. From the observed increase in W-influx and the concomitant increase in the W-concentration in the main plasma, a penetration probability for W eroded from the inner wall to enter the main plasma can be derived [10]. This number is found to be of the order of 1 %,

consistent with modelling using the DIVIMP [37]. The analysis of migration and redeposition patterns is less clear due to the fact that the main W-erosion actually comes from plasma ramp-down when the hot plasma column leans on the inner wall [38].

6. Scenario integration

The physics elements described above are all important steps towards an integrated scenario for ITER. However, the integration itself, i.e. the combination of good confinement, high stability and benign power exhaust at good pumping capability, becomes more and more important, since it is clear that some of the solutions for individual points are not mutually compatible. Therefore, the development of integrated scenarii is a major focus of the ASDEX Upgrade experimental programme.

For the conventional H-mode scenario, the remaining issues are the NTM stability (see section 4.2) and the mitigation of ELM effects on the divertor as addressed in section 4.1. However, recent developments aim at improving the performance above the standard H-mode in view of steady state, i.e. noninductively driven tokamak discharges, the so-called 'Advanced Tokamak' (AT) line. The route of development here is to maximise the fraction of bootstrap current, which requires high β_{pol} and to reduce the total current which requires enhanced confinement, expressed e.g. as $H_{89} = \tau_E/\tau_{E,ITER89}$.

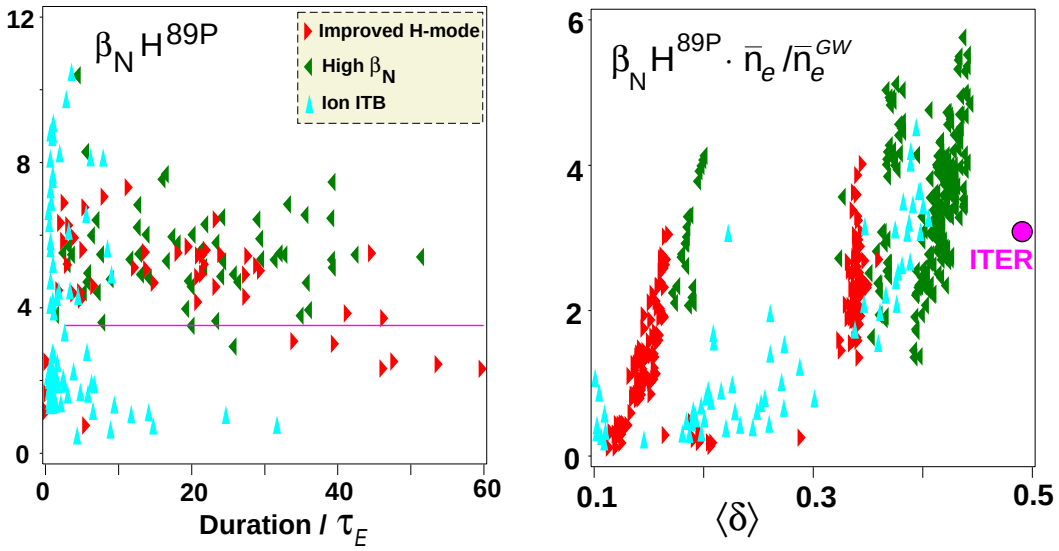

FIG. 10: Performance parameter $\beta_N \times H_{89}$ for various high performance scenarii in ASDEX Upgrade (left). The right figure demonstrates the beneficial effect of increasing δ in achieving higher densities at high performance.

Fig. 10 shows the commonly used figure of merit, $\beta_N H_{89}$, for various ASDEX Upgrade scenarii. As can be seen, ITB scenarii reach very high values, but only for short duration due to the stability limitations discussed in section 3.4. In the so-called 'improved H-mode' and the 'high β_N H-mode', high performance has been achieved in stationary state over many confinement times. In fact, although the highest neutron rate in ASDEX Upgrade is reached in ITB discharges, the highest Q_{equiv} is actually achieved in the 'improved H-mode' [40].

The improved H-mode is characterised by flat central shear and the absence of sawteeth while fishbones maintain the stationarity of the q-profile [39]. The confinement improvement mainly comes from density peaking while the T profiles are still similar to usual H-mode profiles, but with a relatively high pedestal T as boundary condition. A major drawback of this scenario was the limitation to relatively low densities $n_e/n_{GW} \leq 0.5$. As noted before, operation at higher δ allows us to obtain good confinement at high fractions of n_{GW}. Thus, by using higher

δ, it was possible to extend the performance of the 'improved H-mode' regime to $n_e/n_{GW} \approx 0.8-0.9$. Again, these discharges do not have sawteeth and the n_e profile is slightly peaked. Actually, higher δ also proved to be beneficial to lower q_{95} in the improved H-mode regime, which was not possible before due to the onset of sawteeth with lower q_{95}. The degree of peaking can be controlled by central ICRH heating as described in section 3.2. This regime also shows improved stability properties with respect to the improved H-mode regime (with the main limitation being NTM onset) and is called 'high β_N-regime' [41], [42]. It can be obtained in a stationary state at values up to $\beta_N = 3.5$ [43]. This may partly be explained by to the relatively high collisionality, but stability also profits from shaping: increased shaping is expected to affect the stability index Δ', and it allows higher β_N for given β_{pol}, which is the actual quantity limited by NTMs. The beneficial effect of δ is also clearly documented in $\beta_N H_{89} n/n_{GW}$ in the left graph of Fig. 10.

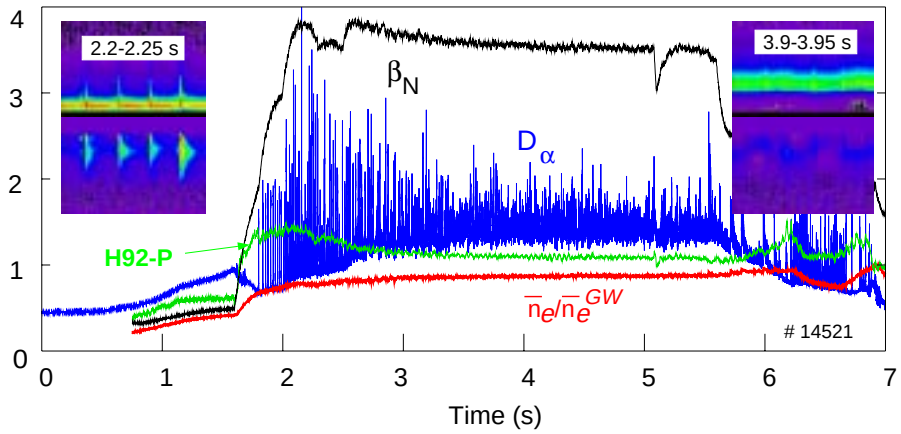

FIG. 11: *High β_N-discharge with type II ELMy edge. The power flux to the divertor plates as shown by the inserts exhibits type I peaks early in the discharge (left), but is continuous later on in the type II phase (right).*

Fig. 11 shows an example of a high β_N discharge. In addition to the favourable performance in steady state, it can also be seen that the conditions for this scenario, i.e. high δ and closeness to double null in combination with high n_e are also compatible with type II ELMs, which can be seen from the plots of deposited power on the target plates: although both frames are obtained in phases with equal heating power, the distinct peaks due to type I ELMs exceed 10 MW/m^2 whereas in the later phase with type II ELMs, the heat flux is continuous and below 5 MW/m^2. For ITER, this scenario therefore shows main advantages compared to the usual H-mode scenario, i.e. the possibility to run at lower I_p and higher bootstrap fraction at similar fusion power (note that P_{fus}/P_{loss} only depends on the ratio H/q), but reduced peak heat flux on the divertor, and therefore to extend the duration of the discharge. However, the bootstrap fraction is still smaller than in an ITB discharge with same β. Therefore, ITB discharges are still the prime candidate for steady state tokamak operation, but the high β_N scenario may be considered an intermediate step on this route.

References

[1] GRUBER, O. et al., *Nucl. Fusion* **41** (2001) 1369.

[2] STÄBLER, A. et al., 29th EPS Conference on Plasma Phys. and Contr. Fusion, Montreux, Switzerland, *ECA*, **26B** (2002) O-5.03.

[3] NGUYEN, F. et al., 29th EPS Conference on Plasma Phys. and Contr. Fusion, Montreux, Switzerland, *ECA*, **26B** (2002) P-1.045.

[4] TARDINI, G. et al., *Nucl. Fusion* **42** (2002) 258.
[5] RYTER, F. et al., this conference IAEA-CN-94 EX/C4-2Ra.
[6] LOPEZ-CARDOSO, N. et al., Plasma Phys. Contr. Fusion, **37** (1995) 799.
[7] TARDINI et al., *Nucl. Fusion* **42** (2002) L11.
[8] STOBER, J. et al., *Nucl. Fusion* **41** (2001) 1535.
[9] STOBER, J. et al., this conference, IAEA-CN-94 EX/C3-7Rb.
[10] NEU, R. et al., *Plasma Phys. Contr. Fusion* **44** (2002) 811.
[11] DUX, R. et al., "Accumulation of Impurities in Advanced Scenarios", accepted for publication in Journal of Nucl. Materials.
[12] NEUHAUSER, J. et al., *Plasma Phys. and Contr. Fusion* **44** (2002), 855.
[13] KALLENBACH, A. et al., this conference, IAEA-CN-94 EX/P4-05.
[14] GREENFIELD, C.M., Phys. Rev. Lett. **86**, (2001), 4544.
[15] SUTTROP, W. et al., "ELM-free stationary H-mode plasmas in the ASDEX Upgrade tokamak", submitted to Plasma Phys. Contr. Fusion.
[16] PEETERS, A.G. et al., this conference, IAEA-CN-94 EX/P4-03.
[17] CONWAY, G.D. et al., *Plasma Phys. Contr. Fusion* **43** (2001) 1239.
[18] STOBER, J. et al., *Nucl. Fusion* **41** (2001) 1123.
[19] GRUBER, O. et al., this conference, IAEA-CN-94 EX/C2-1.
[20] HORTON, L.D., et al., 29th EPS Conference on Plasma Phys. and Contr. Fusion, Montreux, Switzerland, *ECA*, **26B** (2002) P-2.047.
[21] SAARELMA, S. et al., "MHD Stability Analysis of Type II ELMs in ASDEX Upgrade", submitted to Nucl. Fusion.
[22] GREENWALD, M. et al., Phys. Plasmas **6** 1943.
[23] SUTTROP, W. et al., this conference, IAEA-CN-94 EX/P5-07.
[24] SUTTROP, W. et al., 29th EPS Conference on Plasma Phys. and Contr. Fusion, Montreux, Switzerland, *ECA*, **26B** (2002) P-1.030.
[25] LANG, P.T. et al., 29th EPS Conference on Plasma Phys. and Contr. Fusion, Montreux, Switzerland, *ECA*, **26B** (2002) P-1.044.
[26] ZOHM, H. et al., *Phys. Plasmas* **8** (2001) 2009.
[27] GANTENBEIN, G. et al., 29th EPS Conference on Plasma Phys. and Contr. Fusion, Montreux, Switzerland, *ECA*, **26B** (2002) P-1.036.
[28] GÜNTER, S. et al., *Phys. Rev. Lett.* **87** (2001) 275001.
[29] GUDE, A. et al., *Nucl. Fusion* **43** (2002) 833.
[30] STOBER, J. et al., *Plasma Phys. Contr. Fusion* **43** (2001) A39.
[31] MARASCHEK, M. et al., "Stabilisation scaling of neoclassical tearing modes during power rampdowns in ASDEX Upgrade", submitted to Nucl. Fusion.
[32] GÜNTER, S. et al., this conference, IAEA-CN-94 EX/S1-4.
[33] MÜCK, A. et al., 29th EPS Conference on Plasma Phys. and Contr. Fusion, Montreux, Switzerland, *ECA*, **26B** (2002) P-1.037.
[34] PAUTASSO, G. et al., this conference, IAEA-CN-94 EX/P4-14.
[35] R. NEU et al., Plasma Phys. Control. Fusion **44** (2002) 1021.
[36] KRIEGER, K. et al., "Erosion and migration of tungsten employed at the main chamber first wall of ASDEX Upgrade", accepted for publication in Journal of Nucl. Materials.
[37] GEIER, A. et al., "Modeling of Tungsten Transport in the SOL for Sources at the Central Column of ASDEX Upgrade using DIVIMP", accepted for publication in Journal of Nucl. Materials.
[38] ROHDE, V. et al., this conference, IAEA-CN-94 EX/D1-4.
[39] GRUBER, O. et al., *Phys. Rev. Lett.* **83** (1999) 1787.
[40] ZOHM, H. et al., 29th EPS Conference on Plasma Phys. and Contr. Fusion, Montreux, Switzerland, *ECA*, **26B** (2002) P-1.043.
[41] SIPS, A.C.C. et al., *Plasma Phys. Contr. Fusion* **44** (2002) A151.
[42] NA, Y.-S. et al., *Plasma Phys. Contr. Fusion* **44** (2002) 1285.
[43] SIPS, A.C.C., et al., "Steady State Advanced Scenarios at ASDEX Upgrade", accepted for publication in *Plasma Phys. Contr. Fusion* (2002) .